

## A REVIEW OF MULTIPHASE FLOW AND DEPOSITION EFFECTS IN FILM-COOLED GAS TURBINES

by

**Jin WANG<sup>a</sup>, Milan VUJANOVIC<sup>b</sup>, and Bengt SUNDEN<sup>c\*</sup>**

<sup>a</sup>School of Energy and Environmental Engineering, Hebei University of Technology, Tianjin, China

<sup>b</sup>Department of Energy, Power Engineering and Environment,  
Faculty of Mechanical Engineering and Naval Architecture, University of Zagreb, Zagreb, Croatia

<sup>c</sup>Department of Energy Sciences, Division of Heat Transfer, Lund University, Lund, Sweden

Review paper

<https://doi.org/10.2298/TSCI180108258W>

*This paper presents a review of particle deposition research in film-cooled gas turbines based on the recent open literature. Factors affecting deposition capture efficiency and film cooling effectiveness are analyzed. Experimental studies are summarized into two discussions in actual and virtual deposition environments. For investigation in virtual deposition environments, available and reasonable results are obtained by comparison of the Stokes numbers. Recent advances in particle deposition modeling for computational fluid dynamics are also reviewed. Various turbulence models for numerical simulations are investigated, and solutions for treatment of the particle sticking probability are described. In addition, analysis of injecting mist into the coolant flow is conducted to investigate gas-liquid two-phase flow in gas turbines. The conclusion remains that considerable research is yet necessary to fully understand the roles of both deposition and multiphase flow in gas turbines.*

Key words: *film cooling, multiphase flow, deposition, mist, gas turbine*

### Introduction

Gas turbines are important industrial equipment and widely used to provide thermal thrust and produce electric energy. All combustion processes in gas turbines produce pollutants, including NO<sub>x</sub>, CO, and unburned hydrocarbons (UHC), see [1]. As is well-known, the NO<sub>x</sub> is associated with formation of acid rain and depletion of the ozone layer. The CO is one kind of toxic gases, while UHC form smog by combining with NO<sub>x</sub>. A decrease in fuel consumption will reduce CO<sub>2</sub> emissions and slow the speed of global warming. Low temperature at turbine inlets is responsible for the environmental impact. The turbine efficiency is improved by increasing the inlet temperature of gas turbine engines, and the biggest challenge for turbine designers is that the high temperature reduces the service life of hot components [2]. In addition, the inlet temperatures for gas turbines in the real working condition are significantly higher than the values from international standardization organization [3]. In order to improve the operation efficiency and reduce the pollutant emissions, film cooling technique is adopted to protect the vanes/blades from excessive thermal load due to the increase in turbine inlet temperature. During the past half-century, many researchers conducted experi-

\* Corresponding author; e-mail: [bengt.sunden@energy.lth.se](mailto:bengt.sunden@energy.lth.se)

mental tests or numerical simulations for simple configurations without mist injection, *i. e.*, only air film cooling. The blade tip leakage flow and heat transfer were reviewed in a literature survey of cooling techniques from 2001 to 2008 [4]. Film cooling characteristics for various blade locations and computational schemes were investigated by many researchers, *e. g.*, for the leading edge [5], trailing edge cooling [6, 7], and a channel flat wall by considering conjugated heat transfer [8-10]. Generally, the failure prediction of gas turbine blades made of nickel-based alloys was carried out in mechanical metallurgical analyses. Under operating conditions at high temperature, high pressure, and high rotational speed, blade failures can be caused by a number of mechanisms, including thermal fatigue cracking of blades (Mazur *et al.* [11]), hot corrosion of blades (Eliaz *et al.* [12], Salehnasab *et al.* [13]), degradation and erosion of thermal barrier coatings – TBC (Ito *et al.* [14], Wellman and Nicholls [15]), and deposition from the solid and molten particles (Hamed *et al.* [16]). Suspended solid particles are often encountered in a turbomachinery operating environment because of several mechanisms, such as sand storms, eruption of volcanoes, fuel combustion, blowing dust, ice, *etc.* Particulate flow from the eruption of volcanoes is one of the most dangerous environments for aircraft engines. Some researchers investigated the composition and viscosity of volcanic ashes [17], assessed volcanic ash threat to engine performance [18], and deposition rates of volcanic ashes in gas turbines [19]. For studies of the sand blockages, Cardwell *et al.* [20] investigated the negative effect of sand blockages on impingement and film cooling. In addition, particle deposition for land-based engines usually occurs due to the combustion process by burning heavy oils or synthetic fuels. More introduction of advancements in gas turbine fuels was shown in detail in [21]. Effect of biofuel-derived contaminants on coated materials was analyzed by Encinas-Oropesa *et al.* [22]. Measurements of roughness were analyzed for a wide range of land-based turbines [23].

The particles forming the deposition may come from a number of sources, including degradation of upstream components, coal based, dirty synthetic fuels used, incomplete combustion, and airborne particulates from the environment, *etc.* Some researchers are investigating deposition effects of multiphase flow and deposition on heat transfer and film cooling effectiveness. This study aims to review recent experimental and numerical studies for particle deposition in gas turbines.

## **Experimental research on deposition**

### ***Measurements in actual deposition environments***

#### *Ash particulate characterization*

Various particle compositions are used to measure the deposition thickness and structure as shown in tab. 1. The environmental scanning electron microscope was used by Bons *et al.* [24], and they analyzed four ash samples, *i. e.*, coal, pet-coke, straw and sawdust. The used coal was obtained from an operating power plant, and the pet-coke ash is boiler slag from a combined cycle gas turbine power plant. Straw ash was produced in a two-step process: first, volatiles were eliminated; second, the burned ash was cycled through a standard ashing process. The ash particles were grinded to reach the size needed. Crosby *et al.* [25] investigated effects of the coal and pet-coke particles by using the same elemental compositions as shown in [24]. Compared to the data from Ford [26], Jensen *et al.* [27] indicated that the correct ingredients and relative concentrations for the deposition formation can be provided by injecting common dirt into a combustion facility.

**Table 1. Chemical composition of ash particulate (wt.%)**

Author	Year	Na	Mg	Al	Si	P	S	Cl	K	Ca	Ti	V	Mn	Fe	Ni
Bons <i>et al.</i> [24]	2007	6.9	3.6	17.8	47.4	1.6	1.8	0.0	2.6	8.7	1.6	0.0	0.0	6.4	0.0
		4.3	2.2	14.5	38.3	0.0	1.0	0.0	2.5	7.5	0.8	3.4	0.0	22.9	0.9
		1.7	2.54	1.8	48.4	3.4	3.0	2.8	23.4	7.8	0.0	0.0	0.0	5.0	0.0
		5.9	12.4	5.1	11.6	2.2	1.3	0.0	10.7	42.9	1.3	0.0	4.5	1.0	0.0
Crosby <i>et al.</i> [25]	2008	6.9	3.6	17.8	47.4	1.6	1.8	0.0	2.6	8.7	1.6	0.0	0.0	6.4	0.0
		4.3	2.2	14.5	38.3	0.0	1.0	0.0	2.5	7.5	0.8	3.4	0.0	22.9	0.9
Author	Year	SiO <sub>2</sub>	Al <sub>2</sub> O <sub>3</sub>	CaO	MgO	Fe <sub>2</sub> O <sub>3</sub>	FeO	TiO <sub>2</sub>	SrO	SO <sub>3</sub>	K <sub>2</sub> O	Na <sub>2</sub> O			
Ford [26]	1954	59.8	14.9	4.8	3.7	2.7	3.4	–	–	–	–	–			
Jensen <i>et al.</i> [27]	2005	60.2	4.5	13.7	–	10.7	–	–	–	–	–	–			
Smith <i>et al.</i> [28]	2010	32.9	20.3	2.93	–	40.6	–	–	–	0.827	2.48	–			
Bonilla <i>et al.</i> [29]	2012	49.9	11.5	9.4	1.7	14.5	–	3	0.7	1.2	1.6	3.7			
Bonilla <i>et al.</i> [30]	2013	32.8	14.2	31.7	3.6	9.8	–	2.6	1.3	1.2	1.0	0.8			
Webb <i>et al.</i> [31]	2013	32.8	14.2	31.7	3.6	9.8	–	2.6	1.3	1.2	1.0	0.8			
		25.3	13.5	2.3	0.6	52.7	–	1.9	0.1	0.6	2.0	0.3			
		22.1	10.5	42.2	6.9	6.1	–	2.2	0.3	5.7	0.5	1.8			
		49.9	11.5	9.4	1.7	14.5	–	3.0	0.7	1.2	1.6	3.7			

However, the particle sizes were needed to keep consistency with a turbine environment. The bituminous coal ash was used by Smith *et al.* [28] because of the likelihood of being used in synthetic fuels derived from coals. Bonilla *et al.* [29] presented a comparison of film cooling and particle size on ash deposition by using subbituminous fly ash obtained from the Jim Bridger Power Station (JBPS) in Wyoming, USA. A lignite ash from Mississippi were also used to analyze the effect of film cooling on nozzle guide vane deposition (Bonilla *et al.* [30]). Webb *et al.* [31] investigated four coal ash samples, including one ash from a bituminous coal in West Virginia, a lignite ash from Mississippi, two subbituminous fly ash from JBPS and Powder River Basin in Wyoming. Although researchers conducted experimental studies with different particulate compositions from various regions or power stations, formation of the deposition is affected by many critical variables, such as flow temperature, Mach number, impingement angle, chemistry, *etc.*

#### Testing facility for accelerated deposition

Effects of the deposition were investigated mostly based on a turbine accelerated deposition facility (TADF). This facility was developed to simulate the deposition process continuously. Jensen *et al.* [27] earlier presented a description about the TADF facility to provide validation of an accelerated testing principle by using airborne particulate. This facility was designed to simulate 10000 hours turbine operation in a 4 hours deposition test. The TADF was also used in [24] and [32].

A nearly isothermal profile through the target specimen thickness was given, but internal and external cooling schemes are used for modern engines to protect blade materials. In order to obtain a more actual operation conditions, Crosby *et al.* [25] modified a new specimen holder for the TADF facility by considering impingement cooling, and a small fraction of the high pressure air is provided by a particle feed system as shown in fig. 1.

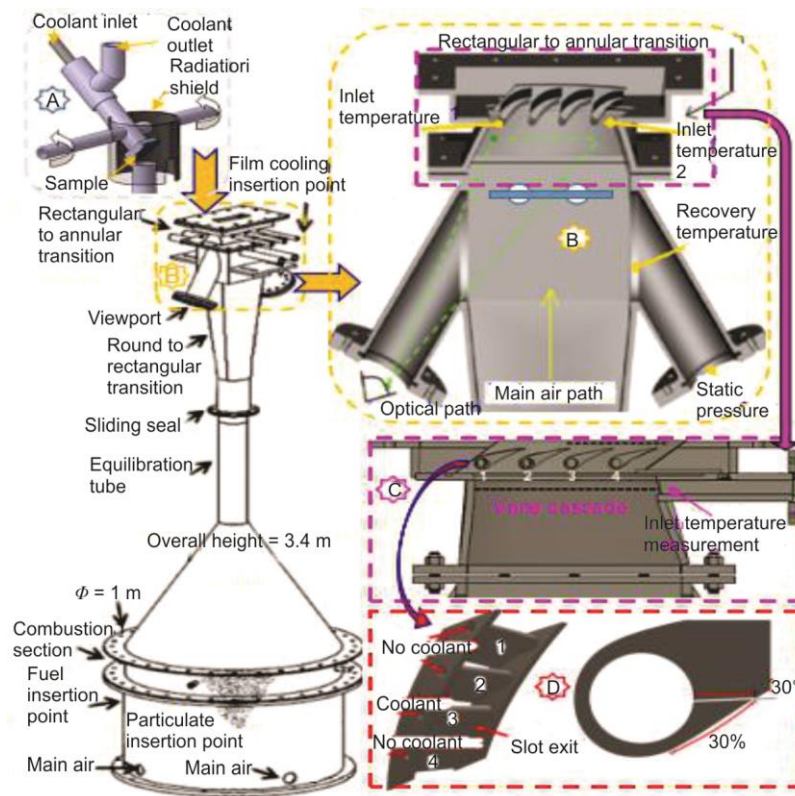


Figure 1. Schematic of turbine reacting flow rig and cooling scheme

Coolant air impinges on the back side of the sample through the center tube, and it is passed by the tube outlet as shown in part A of fig. 1. The specimen holder can be rotated to provide testing measurements at any impingement angle. The developed facility was used in [33, 34]. Considering the deposition on turbine nozzle guide vanes (NGV) by Smith *et al.* [28], two nozzle guide vane doublets were arranged at the outlet of the rectangular annular transition as shown in part B of fig. 1. The NGV were obtained from a CFM56-5B production engine. The developed testing section was named as the turbine reacting flow rig (TuRFR). The air flow was divided into four parts, *i. e.*, mainstream, coolant flow, premix flow, and particulate flow. In addition, two viewing ports on the sides of the TuRFR, and a similar testing facility were also used in [29-31, 35, 36]. Especially, Prenter *et al.* [35] presented the schematic of the annular test section as shown by part C of fig. 1. The vanes are numbered 1-4, and the two center vanes are used to provide periodic flow conditions. In addition, Whitaker *et al.* [37] designed a turbulence grid placed in the flow path upstream the NGV as shown in part D of fig. 1.

The researchers investigated the critical parameters for proper simulation including particle temperature, concentration and residence time. The results indicated that more than twice the deposition rate was obtained by increasing the particle mass mean diameter from 3  $\mu\text{m}$  to 16  $\mu\text{m}$ . and the threshold temperature for deposition was about 960  $^{\circ}\text{C}$ .

### Testing facility for accelerated deposition

Effect of the deposition was investigated by considering the capture efficiency in various references. The capture efficiency was defined as the ratio of the deposition mass on the target surface to the ash mass fed through the system [34]. A formula can be presented to calculate the capture efficiency:

$$\eta_{\text{cap}} = \frac{m_{\text{dep}}}{m_{\text{inject}}} \quad (1)$$

where  $m_{\text{dep}}$  is the deposition mass on the target surface and  $m_{\text{inject}}$  – the total amount of ash injected into the experimental system after completing a test.

For comparison of the capture efficiencies on the NGV, some results were obtained by considering various influence factors, such as particle material [24], particle size [25, 29, 34], gas temperature [25, 34], blowing ratio [33], inlet turbulence level [37], deposition time [34], and hot streak [35, 38, 39]. Effects of the gas temperature and particle size are analyzed in fig. 2.

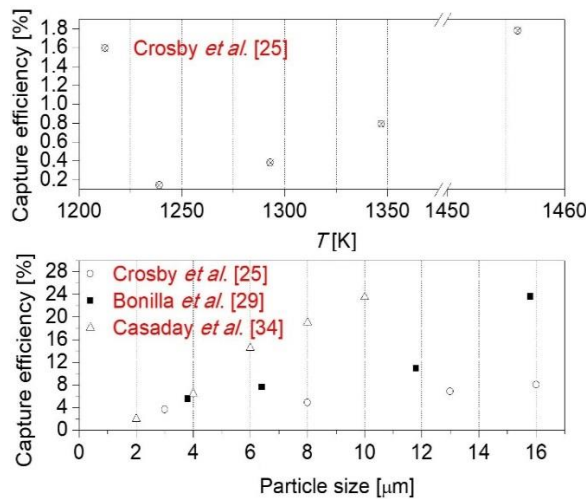


**Figure 2. Effects of the particle size and gas temperature on the capture efficiency**

particle material, the net particle capture efficiency for the coal is obviously higher than for the sawdust and pet-coke [24]. A 76% increase in capture efficiency for the 4.63  $\mu\text{m}$  ash particle was observed with a 50% increase in the freestream turbulence (from approximately 6% to 9%), while an 84% increase for the 6.48  $\mu\text{m}$  particle [37].

The capture efficiency significantly decreased with increasing the blowing ratio. Particles of 13  $\mu\text{m}$  were used to establish a correlation for predicting the deposition development with time. A regressed exponential equation was obtained as follows [34]:

Crosby *et al.* [25] investigated effects of temperature and particle size on deposition in land based turbines. They found that the deposition rate increased with the gas temperature, and an increase above 50% occurred from 1,347 K to 1,456 K. For the studies of the particle size, it was found that the deposition capture efficiency is sensitive to the angle between the coupon and flow turning in the experimental system. The data also indicated that the capture efficiency was less than 10% if the particle size is smaller than 10  $\mu\text{m}$ . Compared to the experimental tests, the simulation results showed a larger deviation due to imperfect computational models. More details will be discussed in a subsequent section of this paper. Considering the

$$\eta_{\text{cap}} = 0.203 e^{0.0529t} + 13.79 \quad (2)$$

### **Measurements in virtual deposition environments**

In order to simulate the deposition process, some methods used in a laboratory were developed by injecting particles into a hot gas path. Sundaram and Thole [40] injected epoxy gel into an aluminum mold to manufacture the deposition. The dried epoxy with sand was sprayed with adhesive to provide a rough deposition surface. They investigated effects of surface deposition, hole blockage, and thermal barrier coating spallation on the end wall film cooling. In addition, Sundaram *et al.* [41] conducted deposition experiments on film cooling of a vane end wall along the pressure side, including studies of single row deposition and multiple row deposition. However, the related references did not explain the difference between the used virtual approach and the actual deposition environment.

### **Matching of actual engine and simulated conditions**

Compared to the epoxy deposition and sand deposition, multiple waxes were chosen to simulate both solid and molten particles. When the Stokes number (Stk) of the experimental study matches that in actual deposition conditions (coal ash particles), the wax particles will show the same behavior in the flow field as coal ash particles do in engine conditions. By matching the Stokes number, the target size for the wax droplets in many studies was calculated and determined by using the formula in Hinds [42]:

$$\text{Stk} = \frac{\tau}{\frac{l_c}{U_c}} = \frac{\rho_p d_p^2 U_c}{18 l_c \mu_g} \quad (3)$$

The Stokes number is a ratio of the time for particles suspended in a fluid-flow,  $\tau$  represents a response of a particle to changes in the fluid flow field, and  $l_c/U_c$  is the time taken for a particle to travel past an obstacle. The deposition is produced slightly for particles with  $\text{Stk} \ll 1$ , while particles with  $\text{Stk} \geq 1$  cannot follow the surrounding flow and more deposits are caused on turbine NGV. More studies concerned the inertial particle deposition with  $\text{Stk} \geq 1$ , so it is very important to match the Stokes numbers in different environment conditions:

$$\text{Stk} = \left( \frac{\rho_p d_p^2 U_c}{18 l_c \mu_g} \right)_{\text{lab}} = \left( \frac{\rho_p d_p^2 U_c}{18 l_c \mu_g} \right)_{\text{engine}} \quad (4)$$

By comparison between engine and wind tunnel conditions, a suitable size of the wax particle is selected. When the particle is made of wax and the other parameters are given, the diameter of the wax particle can be calculated as follows:

$$(d_p)_{\text{wax}} = \sqrt{\left( \frac{\rho_p d_p^2 U_c}{18 l_c \mu_g} \right)_{\text{engine}} / \left( \frac{\rho_p U_c}{18 l_c \mu_g} \right)_{\text{wax}}} \quad (5)$$

For accurate simulations based on the turbine leading edge, the Biot number in laboratory conditions is needed to match actual engine conditions. When the dimensionless thickness ( $b_{\text{wall}}/d$ ) in the laboratory conditions is the same as the actual engine conditions, the Biot numbers can be kept consistent as long as the thermal conductivity ratios satisfy the following formula by Albert and Bogard [43]:

$$\left(\frac{k_{\text{dep}}}{k_{\text{wall}}}\right)_{\text{lab}} \approx \left(\frac{k_{\text{dep}}}{k_{\text{wall}}}\right)_{\text{engine}} \quad (6)$$

### Facility and testing conditions

In Lawson and Thole [44], the deposition process in the vicinity of film cooling holes was observed by using an open loop wind tunnel as shown in fig. 3.

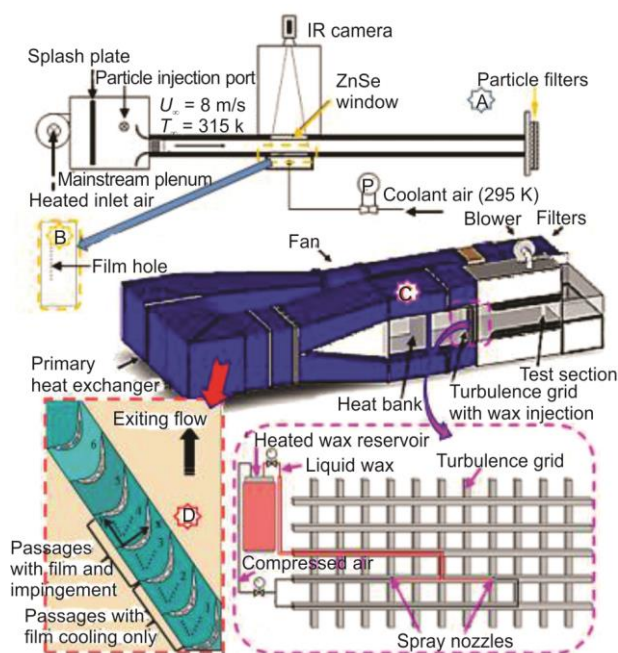


Figure 3. Schematic of an open-loop wind tunnel facility

Mensch and Thole [48] analyzed the combined impingement and film cooling performance in the same linear blade cascade.

Albert and Bogard [43] performed contaminant deposition experiments on a film-cooled turbine airfoil leading edge, and a closed-loop wind tunnel facility was used as shown in fig. 4. The mainstream flow in the wind tunnel was driven by a variable speed fan, and then the flow passed through a water-regulated heat exchanger. After the flow passed by a grid turbulence generator and a wax sprayer in the test section, the mainstream flow passed through an air filter to remove most of the wax particles. A half-cylindrical model was attached to a coolant supply plenum. Davidson *et al.* [49] modified the test section by using a linear cascade with 10×scale model of a C3X vane. The IR thermography was used in order to view the surface temperature distribution of the vane through a NaCl window. The IR camera was calibrated against thermocouples on the vane surface. The vane was covered with TBC, and the TBC also provided a trench depth of above 1-D. Comparison of photographs before and after deposition was conducted in [50]. In addition, Kistenmacher *et al.* [51] studied the effect of contaminant deposition on the realistic trench based on a similar experimental facility.

After the heated room air entered the mainstream plenum through the blower, the mainstream flow mixed with the coolant air in the test section. Coolant air passed by a removable end wall plate with nine film holes. Infrared (IR) thermography was used to acquire a temperature map over the film-cooled end wall, and a removable zinc selenide (ZnSe) window provided maximum transmission to the IR camera. Two particle filters were located at the outlet of the flow channel. A clearer explanation of the experimental facility was shown in [45, 46]. The wax was injected by using a wax particle generator to simulate the deposition process. Liquid wax and the air flow were supplied upstream the test section by a spray nozzle on the turbulence grid. Lawson *et al.* [47] investigated the end wall cooling effectiveness in a cascade with seven blades.

For measurements in virtual deposition environments, particle properties and testing conditions are given in tab. 2. The epoxy gel and the wax particle were common materials used to investigate the deposition in gas turbines. The particle size was calculated by comparison of the Stk numbers in lab experimental conditions and actual deposition conditions. For the lab experiments, the flow velocity of the mainstream was mostly under 10 m/s, and the inlet Mach number is less than 0.3.

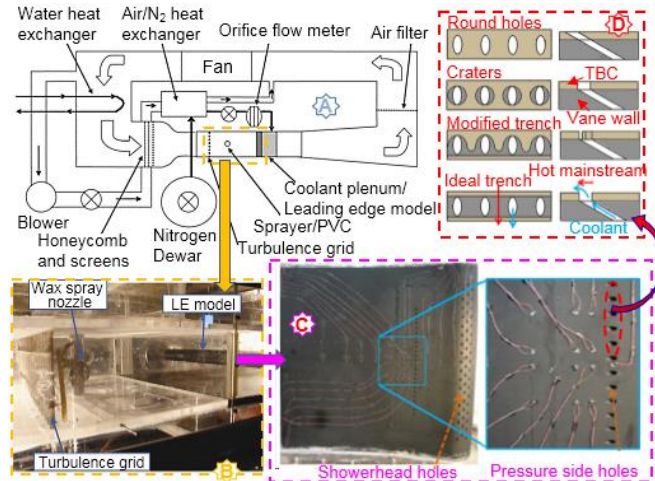


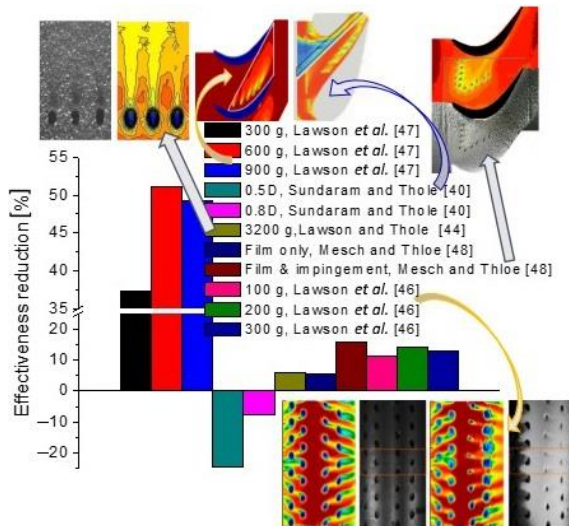
Figure 4. Schematic of a closed-loop wind tunnel facility

Table 2. Particle properties and testing conditions

Author	Particle diam. [ $\mu\text{m}$ ]	Particle density [ $\text{g m}^{-3}$ ]	Mainstream temp. [K]	Mainstream velocity [ $\text{ms}^{-1}$ ]	Inlet Mach number	Inlet Reynolds number	Median Stk	Particle material
Sundaram and Thole [40]	–	–	333	6.3	0.017	$2.1 \cdot 10^5$	–	epoxy
Sundaram et al. [41]	–	–	333	6.3	0.017	$2.1 \cdot 10^5$	–	epoxy
Lawson and Thole [44]	130	900	315	8	–	–	–	wax
Albert and Bogard [43]	8-80	–	294-313	15	–	$4.8 \cdot 10^4$	–	RT31, RT42, wax
Lawson and Thole [45]	1-100	800	338	6.3	0.012	$2.25 \cdot 10^5$	6	wax
Lawson et al. [46]	median 175	800	290, 317	6.68	–	$5.68 \cdot 10^4$	4	wax
Lawson et al. [47]	median 35	800	321, 330	10.4	0.026	$1.25 \cdot 10^5$	6.54	wax
Davidson et al. [50]	10-200	–	301	5.8	–	$7.5 \cdot 10^5$	–	RT31, wax
Kistenmacher et al. [51]	10-100	–	301	5.8	–	$7.5 \cdot 10^5$	–	RT31, wax
Mensch and Thole [48]	median 34	800	320	10.5	0.029	$1.22 \cdot 10^5$	6	wax

#### Effect of deposition on film cooling

In a typical gas turbine, components in the hot gas path operate under hostile conditions. Film cooling is a common technique to protect the turbine components from thermal load. Most researchers investigated the effect of deposition on film cooling effectiveness by



**Figure 5. Reductions of film cooling effectiveness based on deposition surfaces with wax injection,  $M = 1.0$**

using the epoxy and wax materials as shown in fig. 5. For the adiabatic effectiveness tests based on a film-cooled flat end wall, Lawson and Thole [44] investigated 3,200 g deposition (8 cycles) of solid and molten particles at the blowing ratio,  $M$ , of 1.0, and the reduction in film cooling effectiveness,  $\eta$ , reached a maximum of 6%. Lawson *et al.* [47] analyzed reduction of the area-averaged film cooling effectiveness with respect to wax injection mass, including 300 g, 600 g, and 900 g. The results indicated that the film cooling effectiveness with 600 g of the wax injection was reduced by 51%, and this is larger reduction compared to those after 300 g and 900 g of injection. Sundaram and Thole [40] investigated reduction on area-averaged film cooling effectiveness due to surface film cooling distortions. They found that the deposition with heights of 0.5D and 0.8D enhanced the film cooling effectiveness downstream the leading-edge hole row, and the 0.5D deposition height provided a higher increase in film cooling effectiveness compared to the 0.8D deposition height. Mesch and Thole [48] conducted comparison of combined film and impingement at different blowing ratios. The results indicated that the deposition caused a greater reduction in cooling performance for the case with combined film and impingement cooling compared to the case with only film cooling. By using 100 g, 200 g, and 300 g of wax injection, Lawson *et al.* [46] performed experimental research of the deposition effect on the leading-edge film cooling. They found that the largest reduction in effectiveness was observed after just 200 g of wax injection, and there was 2% difference between results from 200 g and 300 g of injection.

Considering comparisons of the results in different references, the area-averaged effectiveness reduction depends on the specific calculation region. For the end wall film cooling, the mass flow rate of the wax injection shows significant influence on effectiveness reduction. Moreover, the effectiveness reduction with more wax injection is usually rising but not monotonously.

### Numerical research on deposition

In order to predict the deposition efficiency and the effect on the film cooling effectiveness, computational fluid mechanics is applied by many researchers. Some critical points need be focused to obtain successful results numerically, including flow modelling and particle tracking.

### Solution to turbulent flow

Considering that turbulent flow is anisotropic, most attempts to predict the flow distribution are based on the solutions of steady Reynolds-averaged Navier-Stokes (RANS), large-eddy simulation (LES) and direct numerical simulations (DNS). The relevant works with turbulence models in recent years are shown in tab. 3.

**Table 3. Deposition predictions in recent numerical methods**

Author	Year	Flow solution	Object	Remarks
Rodgers <i>et al.</i> [53]	2013	DSMC	A stationary airfoil	Coating thickness trends with both substrate surface location and deposition conditions were accurately predicted by using DSMC simulations
Tafti [52]	2005	Quasi-DNS, LES	A ribbed duct for internal cooling	Heat transfer and friction in quasi-DNS calculation cases are under predicted, but the turbulence level in LES calculation increases
Sreedharan <i>et al.</i> [54]	2011	LES	Syngas ash deposition in gas hot path	Discrete phase model (DPM) and discrete random walk (DRW) model based on LES calculations are sensitized to temperature and ash composition
Patil and Tafti [55]	2013	WMLES	A ribbed duct for internal cooling	The wall modelled LES shows more accurate results at higher Reynolds number, and 60-140 times lower computational time than that required for wall resolved LES calculations
Singh <i>et al.</i> [56]	2014	WMLES	Two pass internal-cooled duct	Good agreement with experimental measurements. Results identify the damage prone areas in the internal cooling passages under influence of sand ingestion
Singh and Tafti [57]	2015	WMLES	Sand particle laden jet impacting	The sticking probability is predicted based on the critical viscosity approach and collision losses during a particle-wall collision
Ai and Fletcher [58]	2012	RANS	A coolant plenum	Based on the correlation developed for the particle Young modulus, capture efficiency decreases with increasing the blowing ratio and the hole size
Barker <i>et al.</i> [59]	2013	RANS	GE-E3 NGV	The most deposits on the trailing half of the pressure side and at mid-chord are predicted by the critical viscosity model and the critical velocity model, respectively
Casaday <i>et al.</i> [39]	2012	RANS	GE-E3 NGV	The hot streak results in higher total deposition rates than uniform temperature at the inlet with the same mass-averaged temperature
Casaday <i>et al.</i> [60]	2013	RANS	A cylindrical leading edge and a NGV	Reynolds stress turbulence model better predicts particle tracking in boundary layers and secondary flows than other RANS methods, and the simplified cylindrical leading edge is a valid prediction for end wall deposition
Casaday <i>et al.</i> [38]	2014	RANS	Test regions of TuRFR facility	Computations confirm effects on vane surface temperatures and show peaks in deposition on the vane leading edge
Suman <i>et al.</i> [61]	2013	RANS	A NASA Rotor 37 (compressor stage)	Particles with a diameter of 1 $\mu\text{m}$ results in the most severe deposition condition at the best efficiency point; increasing particle diameter on the pressure side is more affected than on the suction side
Borello <i>et al.</i> [66]	2014	URANS	A wedge-shaped converging duct	A proper and more accurate prediction of the deposit is obtained by using a developed URANS model in an internal cooling channel
Borello <i>et al.</i> [67]	2014	URANS	GE-E3 nozzle vane cascade	Film cooling reduces the total amount of deposition especially along the pressure side
Zagnoli <i>et al.</i> [63]	2015	RANS	GE-E3 nozzle vane cascade	The $k-\omega$ SST turbulence model was employed, and temperature dependent polynomials were specified for the thermal conductivity and specific heat of air
Blunt <i>et al.</i> [64]	2016	RANS	Effusion cooled test coupons at the exit of a stalled diffuser	The $k-\omega$ SST model was used to predicted concentrations of first impacts in the area where deposition was found experimentally

For DNS, the Navier-Stokes equations are numerically solved without any turbulence model, which indicates that the whole range of spatial and temporal scales of the turbulence has to be resolved. All the spatial scales of the turbulence must be associated with the motions containing most of the kinetic energy, and they are resolved in the whole computational domain. Usually, higher order numerical schemes are adopted to reduce the numerical errors. Very large computational resources are necessary to obtain accurate and integral results within a time step. In order to reduce the computational complexity of DNS, quasi-direct numerical simulation (quasi-DNS) was used to investigate internal cooling in a ribbed duct [52]. Generally, a second order central scheme with boundedness has been used for spatial discretization in quasi-DNS. In addition, Rodgers *et al.* [53], simulated the deposition process by using direct simulation monte carlo (DSMC) method. Sreedharan *et al.* [54] found that LES calculations were sensitized to temperature and ash composition for syngas ash deposition in the hot gas path. Patil and Tafti [55], Singh *et al.* [56], Singh and Tafti [57] used the wall modelled LES (WMLES) for simulations of the internal cooling and jet impingement. They confirmed that WMLES provided more accurate results for prediction of the particle deposition.

Based on RANS, the capture efficiency was analyzed in a coolant plenum [58]. For investigation of the particle deposition on NGV, RANS equations are mostly used to predict velocity, temperature fields, and film cooling effectiveness. A similar application has been reported by Casaday *et al.* [38], Casaday *et al.* [39], Barker *et al.* [59] and Casaday *et al.* [60]. In addition, the effect of particle deposition in a compressor stage was also investigated by using RANS [61].

Saha and Acharya [62] concluded that only LES was able to reconstruct the unsteady coherent structures and to affect mixing and heat transfer by analysis of the flow and heat transfer in a rotating rib-roughened duct. However, the great potential of LES in predicting the details of the heat transfer mechanisms cannot counteract the time-consuming disadvantage and the requirement of vast computational resources. Based on a GE-E3 nozzle vane cascade and a stalled diffuser, Zagnoli *et al.* [63] and Blunt *et al.* [64] conducted simulations using the  $k-\omega$  SST turbulence model, respectively. In addition, most studies on turbomachinery CFD generally achieved results by using very crude modeling assumptions based on steady RANS turbulence closure and very simple links between Reynolds stress and velocity gradients [65]. Steady RANS allows affording numerical simulations with a reasonable computational cost, but it often leads to large deviations and questionable results [66]. Therefore, unsteady RANS (URANS) approaches appeared in recent years. URANS aims to recover the well-known deficiencies of basic approaches and to obtain a balance between the simulation accuracy and the computational demands. For example, Borello *et al.* [67] investigated particle laden flows both around a single jet and in a turbine vane cascade by using the URANS method. However, URANS is unable to account for the fluctuations of the flow field, although a transient solution is obtained [68].

From the references in this section, it is concluded that URANS is recommended for deposition research on rotating internal cooling vanes, but RANS with a critical viscosity model is quite common for studies of deposition outside the vanes.

### **Critical viscosity model**

To capture the particle deposition effectiveness numerically, Sreedharan and Tafti [69] presented a critical viscosity model to consider sticking probability. Critical viscosity corresponds to a temperature value above which the viscosity rapidly decreases. It is assumed

that the sticking probability is unity when the viscosity of the particles is at, or below, the critical viscosity. At other temperature it is calculated as a probability function:

$$P_s(T_p) = \frac{\mu_{\text{crit}}}{\mu_{T_p}} \quad (7)$$

where  $\mu_{\text{crit}}$  is the viscosity at the particle at the critical sticking temperature value, and  $\mu_{T_p}$  is the viscosity at the particle at the current temperature value. Ash viscosity was computed as a function of temperature by using a model by Senior and Srinivasachar [70]. Viscosity is calculated based on the equation [71]:

$$\log\left(\frac{\mu}{T_p}\right) = A + \frac{10^3 B}{T_p} \quad (8)$$

where  $A$  and  $B$  are constants which depend on the chemical composition. Further details are described in [70].

### **Critical velocity model**

The impact velocity component normal to the surface is also used to predict whether the particle sticks or reflects. The critical velocity model was completely presented in [59]. The critical velocity is given:

$$V_{\text{cr}} = \left(\frac{2E}{D_p}\right)^{10/7} \quad (9)$$

$$E = 0.51 \left[ \frac{5\pi^2(k_1 + k_2)}{4\rho P^{3/4}} \right]^{2/5} \quad (10)$$

$$k_1 = \frac{1 - \nu_s^2}{\pi E_s} \quad (11)$$

$$k_2 = \frac{1 - \nu_p^2}{\pi E_p} \quad (12)$$

where  $V_{\text{cr}}$  is the critical velocity,  $\nu_s$  is the surface Poisson ratio, and  $\nu_p$  is the particle Poisson ratio.  $E$ ,  $E_s$  and  $E_p$  are Young's moduli of the composite, the surface and the particle, respectively. Particles that impact the surface will deposit when their normal velocities are below the critical velocity. However, particles will reflect off the surface and continue their trajectory when their normal velocities are above the critical impact velocity. To predict the capture efficiency accurately, a function of the Young's modulus was developed in [72]. Moreover, Ai and Fletcher [58] modified the function by considering effect of the surface temperature.

Concerning the critical viscosity model, it has the capability to change the sticking probability with temperature value and ash composition. However, the critical sticking temperature for various ash types should be known before calculation, and the predicted range is dependent on both the temperature and the velocity of the particle as it impacts the surface. For the critical velocity model, it is an obvious deficiency that the viscosity at the critical temperature value cannot be predicted. Despite the deposition models are valid after a correct calibration for Young's modulus or sticking temperature, it can be used for only the initial stages of deposition [59]. Above all, it is necessary to develop or to modify both the critical viscosity and velocity models by further research.

### ***Gas-liquid two-phase flow in film cooling***

Although conventional cooling techniques like air film cooling has significantly contributed to cooling enhancements in the past, it seems that increased net benefits are about to approach its limit. Therefore, some researchers focus on the potential of film-cooling enhancement by injecting mist (water droplets) into the coolant flow, *i. e.*, mist cooling. Mist cooling improves film cooling effectiveness compared to the single-phase film cooling due to the following mechanisms [73]:

- the latent heat of evaporation absorbs large amounts of heat,
- heat transfer from wall significantly increases due to direct contact of liquid droplets with the cooling wall, and
- water droplets and steam have higher specific heats than air.

For the mist cooling, various influential factors for the cooling performance were investigated, including droplet size [73-75], mist concentration [74, 76], mainstream temperature [73, 74], blowing ratio [74, 77, 78], pressure conditions [76], turbulence model [75] and rotation [79]. Li and Wang [75] and Jiang *et al.* [80] investigated mist cooling characteristics near the leading edge based on curved surfaces and on CSX vanes, respectively. In addition, Kanani *et al.* [81] investigated the mist cooling effectiveness by using temperature dependent equations for physical properties.

Cooling performance is significantly enhanced when the mist injection is introduced, and this will reduce the mass flow rate of the cooling air in gas turbines. Although the potential merit in injecting mist into film-cooling flow can be seen easily, a comprehensive investigation of diffusion in gas-liquid flows is needed in detail. In addition, due to potential erosion and corrosion problems concerned by turbine manufacturers, injecting water droplets into the coolant flow has not been widespread in gas turbines.

### **Summary and conclusions**

This paper has reviewed recent research of multiphase flow in gas turbines. The gas-solid two-phase flow, *i. e.*, particulate flow, usually results in corrosion, erosion, and deposition on the components. Experimental studies have shown two primary methods:

- (1) real research method: a TADF is mostly used and developed to simulate the deposition process; the deposition capture efficiency is affected by various factors, including particle material, particle size, blowing ratio, inlet turbulence level, deposition time, *etc.*, and
- (2) virtual research method: the testing particles are made of epoxy, sand and wax instead of real ash particles (like particles derived from coals); reduction of film cooling effectiveness is analyzed in virtual deposition environments; however, the Stokes number in simulated conditions needs to keep the consistency with actual engine conditions; usually, the particle diameter is calculated to match real ash particles.

For numerical simulations by computational fluid mechanics, RANS equations with critical viscosity model are widely adopted to predict the deposition efficiency and the effect on the film cooling effectiveness, comparing to other solutions. Therefore, it is recommended that a more accurate model may be developed based on present sticking models. Mist injection into the coolant flow shows the potential of gas-liquid two-phase flow to enhance the film cooling effectiveness. However, it is limited by possible erosion and corrosion problems. Future studies should take into account both deposition of particles and mist injection.

Considering the harsh operating environments, investigations of the deposition process in film-cooled gas turbines should be further conducted in detail. Such experimental and

simulation methods arouse considerable attention. More developed simulation models should be accurately validated with experimental data in real conditions. Finally, such a study can be favorable for multiphase flow characterizations involved in other industrial applications.

### Acknowledgment

This work is supported by the National Natural Science Foundation of China [Grant No. 51606059].

### Nomenclature

$d_p$  – particle diameter, [m]  
 $M$  – blowing ratio, [ $= \rho_c V_c / \rho_m V_m$ ]  
 $Ma$  – Mach number, [-]  
 $m_{dep}$  – deposition mass, [kg]  
 $m_{inject}$  – injected ash mass, [kg]  
 $Stk$  – Stokes number, [-]  
 $U$  – velocity magnitude, [ $ms^{-1}$ ]  
 $x, y, z$  – co-ordinates, [m]

#### Greek symbols

$\eta$  – adiabatic film cooling effectiveness,  
 [ $= (T_{aw} - T_m) / (T_{jet} - T_m)$ ]

$\eta_{cap}$  – capture efficiency, [-]  
 $\mu$  – dynamic viscosity, [ $kgm^{-1}s^{-1}$ ]  
 $\rho$  – density, [ $kgm^{-3}$ ]

#### Subscripts

aw – adiabatic wall  
 c – coal ash particles  
 jet – coolant jet  
 m – mainstream flow  
 p – particle phase

### References

- [1] Mellor, A. M., Gas Turbine Engine Pollution, *Progress in Energy and Combustion Science*, 1 (1976), 2, pp. 111-133
- [2] Miller, H. E., Nemeč, T. S., *Gas Turbines*, John Wiley and Sons Inc., New York, USA, 2015
- [3] Kostyuk, A. G., Karpunin, A. P., Calculation of Gas Temperature at the Outlet of the Combustion Chamber and in the Air-Gas Channel of a Gas-Turbine Unit by Data of Acceptance Tests in Accordance with ISO, *Thermal Engineering*, 63 (2016), 1, pp. 24-27
- [4] Sunden, B., Xie, G., Gas Turbine Blade Tip Heat Transfer and Cooling: A Literature Survey, *Heat Transfer Engineering*, 31 (2010), 7, pp. 527-554
- [5] Du, K., et al., Effects of the Leading Edge Injection Slot on the Film Cooling and Heat Transfer Performance of the Vane Endwall, *International Journal of Heat and Mass Transfer*, 102 (2016), Nov., pp. 1308-1320
- [6] Xie, Y., Numerical Study on Film Cooling and Convective Heat Transfer Characteristics in the Cutback Region of Turbine Blade Trailing Edge, *Thermal Science*, 20 (2016), Suppl. 3, pp. S643-S649
- [7] Chung, H., et al., Trailing Edge Cooling of a Gas Turbine Blade with Perforated Blockages with Inclined Holes, *International Journal of Heat and Mass Transfer*, 73 (2014), June, pp. 9-20
- [8] Wang, J., et al., Investigations of Film Cooling and Its Nonuniform Distribution for the Conjugate Heat Transfer Passage with a Compound Inclined Angle Jet, *Numerical Heat Transfer, Part A: Applications*, 69 (2016), 1, pp. 14-30
- [9] Wang, J., et al., Conjugated Heat Transfer Analysis of a Film Cooling Passage with Different Rib Configurations, *International Journal of Numerical Methods for Heat & Fluid Flow*, 25 (2015), 4, pp. 841-860
- [10] Wang, J., et al., Conjugated Heat Transfer Analysis of a Film Cooling Passage with Turbulator Ribs, *Heat Transfer Research*, 47 (2016), 2, pp. 89-103
- [11] Mazur, Z., et al., Failure Analysis of a Gas Turbine Nozzle, *Engineering Failure Analysis*, 15 (2008), 7, pp. 913-921
- [12] Eliaz, N., et al., Hot Corrosion in Gas Turbine Components, *Engineering Failure Analysis*, 9 (2002), 1, pp. 31-43
- [13] Salehnasab, B., et al., Hot Corrosion Failure in the First Stage Nozzle of a Gas Turbine Engine, *Engineering Failure Analysis*, 60 (2016), Feb., pp. 316-325
- [14] Ito, A., et al., In-Service Degradation of Metallurgical and Mechanical Properties of Aluminized Coatings and Substrates in Gas Turbine Blades, *Materials Transactions*, 43 (2002), 1, pp. 11-18

- [15] Wellman, R. G., Nicholls, J. R., A Review of the Erosion of Thermal Barrier Coatings, *Journal of Physics D: Applied Physics*, 40 (2007), 16, pp. 293-305
- [16] Hamed, A., et al., Erosion and Deposition in Turbomachinery, *Journal of Propulsion and Power*, 22 (2006), 2, pp. 350-360
- [17] Dean, J., et al., Influence of the Composition and Viscosity of Volcanic Ashes on Their Adhesion within Gas Turbine Aeroengines, *Acta Materialia*, 109 (2016), May, pp. 8-16
- [18] Davison, C. R., Rutke, T. A., Assessment and Characterization of Volcanic Ash Threat to Gas Turbine Engine Performance, *Journal of Engineering for Gas Turbines and Power*, 136 (2014), 8, 81201
- [19] Taltavull, C., et al., Adhesion of Volcanic Ash Particles under Controlled Conditions and Implications for Their Deposition in Gas Turbines, *Advanced Engineering Materials*, 18 (2016), 5, pp. 803-813
- [20] Cardwell, N. D., et al., Investigation of Sand Blocking Within Impingement and Film-Cooling Holes, *Journal of Turbomachinery*, 132 (2010), 2, 21020
- [21] Edwards, T., Advancements in Gas Turbine Fuels From 1943 to 2005, *Journal of Engineering for Gas Turbines and Power*, 129 (2007), 1, pp. 13-20
- [22] Encinas-Oropesa, A., et al., Effect of Biofuel-Derived Contaminants on Coated Industrial Gas Turbines Blade Materials, *Materials and Corrosion*, 65 (2014), 2, pp. 206-216
- [23] Bons, J. P., et al., The Many Faces of Turbine Surface Roughness, *Journal of Turbomachinery*, 123 (2001), 4, pp. 739-748
- [24] Bons, J. P., et al., High-Pressure Turbine Deposition in Land-Based Gas Turbines from Various Synfuels, *Journal of Engineering for Gas Turbines and Power*, 129 (2007), 1, pp. 135-143
- [25] Crosby, J. M., et al., Effects of Temperature and Particle Size on Deposition in Land Based Turbines, *Journal of Engineering for Gas Turbines and Power*, 130 (2008), 5, 51503
- [26] Ford, W. E., *Dana's Textbook of Mineralogy*, John Wiley and Sons, New York, USA, 1954
- [27] Jensen, J. W., et al., Simulated Land-Based Turbine Deposits Generated in an Accelerated Deposition Facility, *Journal of Turbomachinery*, 127 (2005), 3, pp. 462-470
- [28] Smith, C., et al., Deposition in a Turbine Cascade with Combusting Flow, in: *ASME Turbo Expo 2010: Power for Land, Sea, and Air*, Glasgow, UK, 2010, pp. 1-9
- [29] Bonilla, C., et al., The Effect of Particle Size and Film Cooling on Nozzle Guide Vane Deposition, *Journal of Engineering for Gas Turbines and Power*, 134 (2012), 10, 101901
- [30] Bonilla, C., et al., The Effect of Film Cooling on Nozzle Guide Vane Deposition, in: *ASME Turbo Expo 2013: Turbine Technical Conference and Exposition*, San Antonio, Tex., USA, 2013, V03BT13A043
- [31] Webb, J., et al., Coal Ash Deposition on Nozzle Guide Vanes – Part I: Experimental Characteristics of Four Coal Ash Types, *Journal of Turbomachinery*, 135 (2013), 2, 21033
- [32] Wammack, J. E., et al., Evolution of Surface Deposits on a High-Pressure Turbine Blade – Part I: Physical Characteristics, *Journal of Turbomachinery*, 130 (2008), 2, 21020
- [33] Ai, W., et al., Deposition Near Film Cooling Holes on a High Pressure Turbine Vane, *Journal of Turbomachinery*, 134 (2012), 4, 41013
- [34] Laycock, R. G., Fletcher, T. H., Time-Dependent Deposition Characteristics of Fine Coal Fly Ash in a Laboratory Gas Turbine Environment, *Journal of Turbomachinery*, 135 (2012), 2, 21003
- [35] Prenter, R., et al., Deposition on a Cooled Nozzle Guide Vane with Nonuniform Inlet Temperatures, *Journal of Turbomachinery*, 138 (2016), 10, 101005
- [36] Prenter, R., et al., The Effects of Slot Film Cooling on Deposition on a Nozzle Guide Vane, in: *ASME Turbo Expo 2014: Turbine Technical Conference and Exposition*, Dusseldorf, Germany, 2014, V03AT03A017
- [37] Whitaker, S. M., et al., The Effect of Freestream Turbulence on Deposition for Nozzle Guide Vanes, *Journal of Turbomachinery*, 137 (2015), 12, 121001
- [38] Casaday, B., et al., Deposition with Hot Streaks in an Uncooled Turbine Vane Passage, *Journal of Turbomachinery*, 136 (2013), 4, 41017
- [39] Casaday, B., et al., Effect of Hot Streaks on Ash Deposition in an Uncooled Turbine Vane Passage, in: *50<sup>th</sup> AIAA Aerospace Sciences Meeting*, Nashville, Tenn., USA, 2012, pp. 1-22
- [40] Sundaram, N., Thole, K. A., Effects of Surface Deposition, Hole Blockage, and Thermal Barrier Coating Spallation on Vane Endwall Film Cooling, *Journal of Turbomachinery*, 129 (2007), 3, pp. 599-607
- [41] Sundaram, N., et al., Effects of Deposits on Film Cooling of a Vane Endwall Along the Pressure Side, *Journal of Turbomachinery*, 130 (2008), 4, 41006
- [42] Hinds, W., *Aerosol Technology: Properties, Behavior, and Measurement of Airborne Particles*, Wiley-Interscience, New York, USA, 1999

- [43] Albert, J. E., Bogard, D. G., Experimental Simulation of Contaminant Deposition on a Film Cooled Turbine Airfoil Leading Edge, *Journal of Turbomachinery*, 134 (2012), 5, 51014
- [44] Lawson, S. A., Thole, K. A., Effects of Simulated Particle Deposition on Film Cooling, *Journal of Turbomachinery*, 133 (2011), 2, 21009
- [45] Lawson, S. A., Thole, K. A., Simulations of Multiphase Particle Deposition on Endwall Film-Cooling Holes in Transverse Trenches, *Journal of Turbomachinery*, 134 (2012), 5, 51040
- [46] Lawson, S. A., et al., Simulations of Multiphase Particle Deposition on a Showerhead With Staggered Film-Cooling Holes, *Journal of Turbomachinery*, 134 (2012), 5, 51041
- [47] Lawson, S. A., et al., Simulations of Multiphase Particle Deposition on a Nonaxisymmetric Contoured Endwall with Film-Cooling, *Journal of Turbomachinery*, 135 (2013), 3, 31032
- [48] Mensch, A., Thole, K. A., Simulations of Multiphase Particle Deposition on a Gas Turbine Endwall with Impingement and Film Cooling, *Journal of Turbomachinery*, 137 (2015), 11, 111002
- [49] Davidson, F. T., et al., Film Cooling with a Thermal Barrier Coating: Round Holes, Craters, and Trenches, *Journal of Turbomachinery*, 136 (2013), 4, 41007
- [50] Davidson, F. T., et al., A Study of Deposition on a Turbine Vane with a Thermal Barrier Coating and Various Film Cooling Geometries, *Journal of Turbomachinery*, 136 (2014), 4, 41009
- [51] Kistenmacher, D. A., et al., Realistic Trench Film Cooling with a Thermal Barrier Coating and Deposition, *Journal of Turbomachinery*, 136 (2014), 9, 91002
- [52] Tafti, D., Evaluating the Role of Subgrid Stress Modeling in a Ribbed Duct for the Internal Cooling of Turbine Blades, *International Journal of Heat and Fluid Flow*, 26 (2005), 1, pp. 92-104
- [53] Rodgers, T. M., et al., Thermal Barrier Coating Deposition by Rarefied Gas Jet Assisted Processes: Simulations of Deposition on a Stationary Airfoil, *Journal of Vacuum Science & Technology A: Vacuum, Surfaces, and Films*, 31 (2013), 6, pp. 61509
- [54] Sreedharan, S. S., Tafti, D., Composition Dependent Model for the Prediction of Syngas Ash Deposition in Turbine Gas Hotpath, *International Journal of Heat and Fluid Flow*, 32 (2011), 1, pp. 201-211
- [55] Patil, S., Tafti, D., Large-Eddy Simulation with Zonal near Wall Treatment of Flow and Heat Transfer in a Ribbed Duct for the Internal Cooling of Turbine Blades, *Journal of Turbomachinery*, 135 (2013), 3, 31006
- [56] Singh, S., et al., Sand Transport in a Two Pass Internal Cooling Duct with Rib Turbulators, *International Journal of Heat and Fluid Flow*, 46 (2014), Apr., pp. 158-167
- [57] Singh, S., Tafti, D., Particle Deposition Model for Particulate Flows at High Temperatures in Gas Turbine Components, *International Journal of Heat and Fluid Flow*, 52 (2015), Apr., pp. 72-83
- [58] Ai, W., Fletcher, T. H., Computational Analysis of Conjugate Heat Transfer and Particulate Deposition on a High Pressure Turbine Vane, *Journal of Turbomachinery*, 134 (2012), 4, 41020
- [59] Barker, B., et al., Coal Ash Deposition on Nozzle Guide Vanes – Part II: Computational Modeling, *Journal of Turbomachinery*, 135 (2012), 1, 11015
- [60] Casaday, B. P., et al., Numerical Investigation of Ash Deposition on Nozzle Guide Vane Endwalls, *Journal of Engineering for Gas Turbines and Power*, 135 (2013), 3, 32001
- [61] Suman, A., et al., Quantitative Computational Fluid Dynamic Analyses of Particle Deposition on a Transonic Axial Compressor Blade – Part II: Impact Kinematics and Particle Sticking Analysis, *Journal of Turbomachinery*, 137 (2014), 2, 21010
- [62] Saha, A. K., Acharya, S., Flow and Heat Transfer in an Internally Ribbed Duct with Rotation: An Assessment of Large Eddy Simulations and Unsteady Reynolds-Averaged Navier-Stokes Simulations, *Journal of Turbomachinery*, 127 (2005), 2, pp. 306-320
- [63] Zagnoli, D., et al., Numerical Study of Deposition in a Full Turbine Stage Using Steady and Unsteady Methods, in: *ASME Turbo Expo 2015: Turbine Technical Conference and Exposition*, Montreal, Canada, 2015, V02CT44A026
- [64] Blunt, R., et al., The Effects of Turning Angle on Particle Deposition in Turbine Cooling Holes, in: *46<sup>th</sup> AIAA Fluid Dynamics Conference*, Washington, D. C., USA, 2011
- [65] Donahoo, E. E., et al., Determination of Optimal Row Spacing for a Staggered Cross-Pin Array in a Turbine Blade Cooling Passage, *Journal of Enhanced Heat Transfer*, 8 (2001), 1, pp. 41-53
- [66] Borello, D., et al., Unsteady RANS Analysis of Particles Deposition in the Coolant Channel of a Gas Turbine Blade Using a Non-Linear Model, in: *ASME Turbo Expo 2014: Turbine Technical Conference and Exposition*, Dusseldorf, Germany, 2014, V05AT12A035
- [67] Borello, D., et al., Study of Particles Deposition in Gas Turbine Blades in Presence of Film Cooling, in: *ASME Turbo Expo 2014: Turbine Technical Conference and Exposition*, Dusseldorf, Germany, 2014, V05BT13A043

- [68] Salim, S. M., et al., Comparison of RANS, URANS and LES in the Prediction of Airflow and Pollutant Dispersion, *Proceedings*, World Congress on Engineering and Computer Science, San Francisco, Cal., USA, 2011
- [69] Sreedharan, S. S., Tafti, D., Composition Dependent Model for the Prediction of Syngas Ash Deposition with Application to a Leading Edge Turbine Vane, in: *ASME Turbo Expo 2010: Power for Land, Sea and Air*, Glasgow, UK, 2010
- [70] Senior, C. L., Srinivasachar, S., Viscosity of Ash Particles in Combustion Systems for Prediction of Particle Sticking, *Energy & Fuels*, 9 (1995), 2, pp. 277-283
- [71] Urbain, G., et al., Viscosity of Silicate Melts, *Transactions and Journal of the British Ceramic Society*, 80 (1981), 4, pp. 139-141
- [72] El-Batsh, H., Modeling Particle Deposition on Compressor and Turbine Blade Surfaces Modeling Particle Deposition on Compressor and Turbine Blade Surfaces, Ph. D. thesis, Vienna University of Technology, Vienna, Austria, 2001
- [73] Li, X., Wang, T., Simulation of Film Cooling Enhancement with Mist Injection, *Journal of Heat Transfer*, 128 (2006), 6, pp. 509-519
- [74] Wang, J., et al., Two-Phase Flow Simulation of Mist Film Cooling with Deposition for Various Boundary Conditions, *Numerical Heat Transfer, Part A: Applications*, 71 (2017), 9, pp. 895-909
- [75] Li, X., Wang, T., Two-Phase Flow Simulation of Mist Film Cooling on Turbine Blades with Conjugate Internal Cooling, *Journal of Heat Transfer*, 130 (2008), 10, 102901
- [76] Wang, T., Li, X., Mist Film Cooling Simulation at Gas Turbine Operating Conditions, *International Journal of Heat and Mass Transfer*, 51 (2008), 21-22, pp. 5305-5317
- [77] Wang, J., et al., Effects of Deposition Locations on Film Cooling with and without a Mist Injection, *Numerical Heat Transfer, Part A: Applications*, 70 (2016), 10, pp. 1072-1086
- [78] Wang, J., et al., Effect of an Upstream Bulge Configuration on Film Cooling with and without Mist Injection, *Journal of Environmental Management*, 203 (2017), Part 3, pp. 1072-1079
- [79] Dhanasekaran, T. S., Wang, T., Simulation of Mist Film Cooling on Rotating Gas Turbine Blades, *Journal of Heat Transfer*, 134 (2012), 1, 11501
- [80] Jiang, Y., et al., Numerical Simulation on Turbine Blade Leading-Edge High-Efficiency Film Cooling by the Application of Water Mist, *Numerical Heat Transfer, Part A: Applications*, 66 (2014), 12, pp. 1341-1364
- [81] Kanani, H., et al., Numerical Modelling of Film Cooling with and without Mist Injection, *Heat and Mass Transfer*, 45 (2009), 6, pp. 727-741